

Research Article

Ferroptosis-related Gene Glutathione Peroxidase 4 Promotes Reprogramming of Glucose Metabolism via Akt-mTOR Axis in Intrahepatic Cholangiocarcinoma

5 **Authors:**

Yutaro HORI ^a, Tomoaki YOH ^a, Hiroto NISHINO ^a, Keisuke OKURA ^a, Makoto KURIMOTO ^a, Yuichi TAKAMATSU ^a, Motohiko SATOH ^a, Takahiro NISHIO ^a, Yukinori KOYAMA ^a, Takamichi ISHII ^a, Keiko IWAIKAWA ^b, Satoru SEO ^c, and Etsuro HATANO ^a

10 **Affiliations:**

^a Department of Surgery, Graduate School of Medicine, Kyoto University, Kyoto, Japan

^b Department of Medical Life Systems, Faculty of Life and Medical Science, Doshisha University, Kyotanabe, Japan

^c Department of Surgery, Faculty of Medicine, Kochi Medical School, Nankoku, Japan

15

Corresponding Author:

Tomoaki Yoh, MD, PhD

Department of Surgery, Graduate School of Medicine, Kyoto University

54 Kawahara-cho, Shogoin, Sakyo-ku, Kyoto 606-8507, Japan

20 Tel: +81-75-751-4323, Fax: +81-75-751-4263

E-mail: tomyoh@kuhp.kyoto-u.ac.jp

ABSTRACT

The role of the ferroptosis-related gene glutathione peroxidase 4 (GPX4) in oncology has been extensively investigated. However, the clinical implications of GPX4 in patients with intrahepatic cholangiocarcinoma (ICC) remain unknown. This study aimed to evaluate the prognostic impact of GPX4 and its underlying molecular mechanisms in patients with ICC. Fifty-seven patients who underwent surgical resection for ICC between 2010 and 2017 were retrospectively analyzed. Based on the immunohistochemistry, patients were divided into GPX4 high (n=15) and low (n=42) groups, and clinical outcomes were assessed. Furthermore, the roles of GPX4 in cell proliferation, migration, and gene expression were analyzed in ICC cell lines *in vitro* and *vivo*. The results from clinical study showed that GPX4 high group showed significant associations with high SUVmax on ¹⁸F-FDG-PET (≥ 8.0 , $p=0.017$), multiple tumors ($p=0.004$), and showed GLUT1 high expression with a trend towards significance ($p=0.053$). Overall and recurrence-free survival in the GPX4 high expression group were significantly worse than those in the GPX4 low expression group ($p=0.038$ and $p<0.001$, respectively). In the experimental study, inhibition of GPX4 attenuated cell proliferation and migration in ICC cell lines. Inhibition of GPX4 also decreased the expression of glucose metabolism-related genes, such as *GLUT1* or *HIF1 α* . Mechanistically, these molecular changes are regulated in Akt-mTOR axis. In conclusion, this study suggested the pivotal value of GPX4 serving as a prognostic marker for patients with ICC. Furthermore, GPX4 can mediate glucose metabolism of ICC.

SUMMARY

GPX4 is acknowledged as a regulator of ferroptosis. This study assessed the prognostic significance of GPX4 and its molecular mechanisms in intrahepatic cholangiocarcinoma. GPX4 is a prognostic marker for these patients, and mediates glucose metabolism through Akt-mTOR axis.

5

KEYWORDS

Intrahepatic cholangiocarcinoma, Glutathione peroxidase 4 (GPX4), mTOR, ferroptosis

SHORT TYTLE

10 GPX4 and glucose metabolism in ICC

15

20

INTRODUCTION

Intrahepatic cholangiocarcinoma (ICC) is the second most common primary liver cancer, accounting for 5–15% of primary liver cancers, and the number of patients with ICC is increasing worldwide [1, 2]. However, limited patients are candidates for surgical resection, which is the mainstay of curative treatment for ICC [3]. Additionally, the postoperative recurrence rate is 50–60% [4]. Recently, several studies have revealed that 5-fluorouracil based adjuvant chemotherapy can prolong postoperative survival [5, 6]. While these evidences may shed light on patients with ICC, the survival outcome in these patients remains unsatisfactory, and novel anticancer therapies are required.

Ferroptosis is a new type of regulated cell death characterized by iron-dependent regulation and generation of reactive oxygen species (ROS), and is different from other conventional cell death [7, 8]. Ferroptosis-related gene, glutathione peroxidase 4 (GPX4) is a critical rate-limiting factor of ferroptosis in the regulation of intracellular ROS that degrade intracellular lipid peroxides into lipid alcohol [9]. Recently, several studies investigated the oncological role of GPX4 in some cancer cells, and identified that the inhibition of GPX4 using GPX4 inhibitor or gene silencing attenuated tumor progression [10-12]. These findings provide the pivotal role of GPX4 to be involved in tumorigenesis and GPX4 might be a novel anti-cancer therapeutic target. However, the clinical implication and the pathophysiologic role of GPX4 on tumorigenesis in ICC remain unclear.

The aim of this study was to determine whether GPX4 has a prognostic impact on survival outcomes in patients with ICC who underwent surgical resection. Furthermore, we investigated the pathophysiological role of GPX4 in the tumorigenesis using the ICC cell lines.

MATERIAL AND METHODS

Study design

This study consisted of clinical and experimental studies investigating the prognostic impact and the role of GPX4 in patients with ICC after surgical resection. The study involved the following steps: i) assessing the expression of GPX4 by immunohistochemistry (IHC) using surgical specimens and
5 investigating the clinical characteristics and prognostic value of GPX4 in patients with ICC after surgical resection and ii) validating the pathophysiological role and molecular mechanism of GPX4 in tumorigenesis *in vitro* and *vivo*.

Clinical study

10 This clinical study aimed to assess whether GPX4 has a prognostic impact on patients with ICC after surgical resection. The study was approved by the Ethics Committee of Kyoto University Hospital, Graduate School, and Faculty of Medicine (No. R3808), and the Opt-out informed consent was used for use of participant data for research purposes.

We retrospectively reviewed an institutional medical database of patients who underwent
15 hepatectomy in Department of Surgery, Kyoto University, between 2010 and 2017, and selected 64 consecutive patients who were pathologically diagnosed with ICC. The final diagnosis was histologically confirmed by at least two experienced hepatobiliary pathologists. Based on the IHC assessment of GPX4 expression, patients were divided into GPX4 high and low groups. The cut-off value of GPX4 was determined using a method described later.

20 Clinicopathological and survival data were obtained from a prospectively maintained institutional database. Tumor characteristics and surgical margins were evaluated based on the final pathological diagnosis. The cut-off value of tumor standardized uptake value (SUVmax) ≥ 8.0 was

previously reported [13]. The tumor stage was assessed by the 8th edition of the American Joint Committee on Cancer (AJCC) classification [14]. Regarding the postoperative complications, grade \geq II complications according to the Clavien-Dindo classification [15] were recorded. The follow-up data were updated as of April 2023. The treatment strategy for ICC in our department was previously reported [13, 16, 17].

Immunohistochemistry

GPX4 and glucose transporter 1 (GLUT1) expression were evaluated by IHC. Briefly, formalin-fixed, paraffin-embedded 4- μ m thick sections were incubated with primary antibody at 4 °C overnight (**SUPPLEMENTARY TABLE 1**). EnVision Polymer (DAKO), a horseradish peroxidase-labeled polymer-conjugated anti-rabbit IgG antibody, was used as the secondary antibody. The samples were stained using diaminobenzidine solution (DAKO) and hematoxylin for counterstaining.

Cell culture and Reagents

Three types of human ICC cell lines: HuCCT-1, RBE, and Huh28 were provided by the Japanese Collection of Research Bioresources Cell Bank (Osaka, Japan). A human ICC: SSP-25 and a human hepatocellular carcinoma (HCC) cell line: Huh7 were provided by the RIKEN Bioresource Center (Tsukuba, Japan). All cell lines were authenticated by bacterial testing, mycoplasma screening, and STR analysis prior to providing the cell banks in 2017. These cell lines were cultured in RPMI 1640 medium supplemented with 10% fetal bovine serum and 1% penicillin and streptomycin at 37 °C in the incubator in 5% CO₂.

(1S,3R)-RSL3 (RSL3; 19288) was purchased from Cayman Chemical, AZD8055 (AZD; S1555) and MHY1485 (MHY; S7811) was purchased from Selleckchem. All the reagents were dissolved in the appropriate buffer according to the manufacturer's protocol. Gene silencing was performed by transfecting ICC cells with GPX4-siRNA (sc-44465; Santa Cruz Biotechnology) or control-siRNA (sc-37007; Santa Cruz Biotechnology) using a transfection reagent (sc-29528; Santa Cruz Biotechnology). To confirm the off-target effects of siRNA, mRNA and protein expression were validated using individual siRNAs (sc-44465A and sc-44456B; Santa Cruz Biotechnology) in one component.

Cell proliferation and migration assay

Cell proliferation was measured by the WST-8 assay using Cell Counting Kit-8 (CCK8; DOJINDO Laboratories). To measure cell proliferation, 5,000 cells of SSP-25 and HuCCT-1 per well were seeded in 96-well plates and treated with the reagents. After incubation, 10 μ L of CCK8 solution was added into each well and incubated at 37 °C for 1.5 h. The absorbance of the plates was read at 450 nm using a microplate reader. Relative proliferation rate was defined as the ratio of absorbance at 450 nm in cells treated with the reagent to that in control cells. To enhance the reproducibility of the cell proliferative assay, CyQUANT NF Cell Proliferative Assay Kit (Invitrogen) was also applied to assess the cell proliferation. Briefly, 5,000 cells per well were seeded in 96-well plates and treated with the reagents. After the incubation for 72 h, 100 μ L of dye binding solution was dispensed and additionally incubated at 37 °C for 30 min. The fluorescence intensity was read by a fluorescence microplate reader (excitation wavelength, 485 nm; emission wavelength, 530 nm). Relative proliferative potential was calculated by comparing the intensity of control cells.

Migration was examined using a wound-healing assay. Briefly, ICC cells with confluency in 6-well plates were scratched using sterile 200 μ L pipette tips. The cells were then treated with the

reagents and incubated for 12 and 24 h, and the distance of the wound was measured using an inverted microscope (SHIMADZU) at 40x magnification. The migration rate was calculated by comparing baseline measurements.

5 **Cell viability assay**

Cell viability was assessed using Cellstain double staining kit (DOJINDO Laboratories). Briefly, ICC cells were treated with 10 μ M of RSL3 or DMSO, and the cell suspensions were prepared as a concentration for 2.0×10^6 /ml. The cell suspensions were incubated with a mixture of Calcein-AM (staining viable cells) and PI (staining dead cells) for 15 minutes. After incubation, cells were observed
10 under a fluorescence microscopy, and Calcein-AM and PI positive cells were calculated.

Western blot

Protein levels were examined by immunoblotting. Briefly, 10 μ g of samples were loaded and subjected to electrophoresis on 10-20% sodium dodecyl sulfate-polyacrylamide gel electrophoresis
15 (ATTO) for 1–2 h to separate the target protein. After transferring the protein to nitrocellulose membrane (GE Healthcare) and blocking for 0.5-1 h using Blocking one (Nacalai Tesque), the membrane was incubated with primary antibody (**SUPPLEMENTARY TABLE 1**) at 4°C overnight. The blot was observed using EZ-capture II (ATTO) after visualization by ECL Prime (GE Healthcare). Actin was used as the loading control.

20

qRT-PCR

Total RNA was isolated from cells using TRIzol reagent (Thermo Fisher Scientific) and purified using RNeasy Mini Kit (Qiagen). Then, cDNA was synthesized using Omniscript RT Kit (Qiagen), and subjected to qRT-PCR using StepOnePlus Real-Time PCR System (Applied Biosystems) and Fast SYBR Green Master Mix (Applied Biosystems). The expression levels of target genes were normalized against GAPDH using the $\Delta\Delta C_t$ method. Primers used in the experiments are listed in **SUPPLEMENTARY TABLE 2.**

Tumor xenograft model

Six- to seven-week-old nude mice (KSN/Slc) were purchased from Japan SLC (Shizuoka, Japan) and used as recipients for xenotransplantation. The cell suspension was prepared as a total of 1.0×10^7 HuCCT-1 cells in 0.5 mL of phosphate-buffered saline (PBS) and 0.5 mL of Matrigel Matrix (BD Biosciences), and 100 μ L of cell suspension was subcutaneously injected into the flank. One week after transplantation, the mice were divided into two groups: RSL3 treatment (RSL3 dissolved in 5% dimethyl sulfoxide (DMSO) and PBS to a concentration of 100 mg/kg, n=6) and control (5% DMSO and PBS only, n=5) groups. The reagents were injected at the same site as the transplantation. The injection of RSL3 or control was repeated twice per week. Tumor size was measured weekly after treatment initiation. The tumor volume was calculated using the following formula: length (width)² x 0.52. Mice were sacrificed 5 weeks after inoculation and subcutaneous tumors were harvested.

Statistical analyses

Data from human clinical samples were analyzed as follows. Categorical variables were expressed as numbers and percentages, and compared using the chi-square test and Fisher's exact test, as

appropriate. Continuous variables were expressed as median values and ranges, and were compared using the Mann–Whitney U test. To evaluate GPX4 and GLUT1 expression by IHC, tumor cells with strongly positive staining were counted in 10 fields (200 × magnification) and the mean percentages were calculated. The cut-off value for GPX4 and GLUT1 expression was determined using the minimum p value approach for overall survival (OS) [18, 19]. The cut-off values for GPX4 and GLUT1 expression were adjusted in increments of 5%. OS was calculated from the date of surgery to the date of death or the end of follow-up, and recurrence-free survival (RFS) was calculated from the date of surgery to the date of death or recurrence. Survival and recurrence rates were estimated using the Kaplan–Meier method and compared using the log-rank test. Cox proportional hazards modeling (stepwise backward model) was used to analyze the factors associated with OS and RFS in univariate and multivariate analyses. When collinearity was encountered, a choice was made based on clinical reasoning. A value of $p < 0.05$ was considered statistically significant.

Data from *in vitro* and *vivo* experiments were analyzed using Student’s t -test and expressed as mean \pm SD. All statistical analyses were performed using JMP version 15.

RESULTS

Clinical Study

Clinical characteristics of GPX4 over-expression in patients with ICC after surgical resection

First, we evaluated the prognostic value of GPX4 expression in patients with ICC after surgical resection. There were 64 consecutive patients with ICC who underwent surgical resection at Kyoto University between 2010 and 2017, and GPX4 expression was measured by IHC in surgical specimens from these patients. Of these, four patients with postoperative mortality and three patients with No.

16 lymph node metastasis were excluded, and 57 patients were investigated. In this population, 36 patients (63.2%) had advanced disease (AJCC stage III/IV), 50 patients (87.7%) underwent major hepatectomy, and 36 patients (63.2%) received adjuvant chemotherapy (**SUPPLEMENTARY TABLE 3**). The median OS was 32.0 months, and the 5-year OS rate was 34.3%. The median RFS was 13.0 months, and the 5-year RFS rate was 16.2%, respectively.

An IHC identified varying degrees of cytoplasmic GPX4 expression in cancer cells (**FIGURE 1A**). The cut-off value for GPX4 expression was determined using the minimum p value approach with 5% increments; the minimum p values were observed when 65% of cells were positive for GPX4. Based on the IHC results, patients were divided into two groups: GPX4 high (n=15) and low expression (n=42), respectively. Patients with GPX4 high expression was significantly associated with hepatitis C infection ($p=0.036$) and multiple tumors ($p=0.004$) (**TABLE 1**).

Association of GPX4 expression with ^{18}F -FDG uptake and GLUT1 expression

Previous studies have revealed that multiple tumors were correlated with SUVmax high in patients with ICC [16, 17]. SUVmax is a parameter of ^{18}F -fluorodeoxyglucose-positron emission tomography (^{18}F -FDG-PET) and a surrogate marker of glucose metabolism, including GLUT1 and hypoxia-inducible factor-1 (HIF1 α) in cancer cells [20, 21]. Therefore, the associations between GPX4, SUVmax, and GLUT1 expression were investigated. Among the patients for whom data of ^{18}F -FDG-PET were available (n=51), patients with GPX4 high expression were significantly associated with SUVmax high ($p=0.017$) (**FIGURE 1B, and TABLE 2**). Indeed, GLUT1 high expression (i.e., 50% determined by minimum p value approach, **SUPPLEMENTARY FIGURE 1A**) showed GPX4 high expression ($p=0.053$) with trend towards significance (**TABLE 2**). These glucose metabolism-related makers also

significantly stratified postoperative survival outcomes in patients with ICC (**SUPPLEMENTARY FIGURE 1B-E**).

GPX4 over-expression stratified survival outcomes in patients with ICC after surgical resection

5 Regarding the survival outcomes, OS was significantly shorter in patients with GPX4 high expression than in those with GPX4 low expression ($p=0.038$) (**FIGURE 1C**). The median OS and the 5-year OS rates of the GPX4 high and low expression groups were 28.0 months versus 53.2 months, and 15.3% versus 39.6%, respectively. Furthermore, RFS was significantly shorter in patients with GPX4 high expression than in those with GPX4 low expression ($p<0.001$) (**FIGURE 1D**). The median RFS and the
10 1-year RFS rates of GPX4 high and low expression groups were 6.5 months versus 23.3 months, and 32.0% versus 68.3%, respectively. Next, multivariate analyses were performed to assess the prognostic impact of GPX4 expression. Among the reported prognostic factors, multiple tumors were excluded from the analyses because of their correlation with GPX4 expression (**TABLE 1**). Multivariate analysis showed that microvascular invasion ($p=0.003$) and GPX4 levels ($p=0.049$) were significant
15 predictors of OS (**SUPPLEMENTARY TABLE 4**). Furthermore, the prognostic significance of GPX4 was retained with respect to RFS ($p=0.002$) (**SUPPLEMENTARY TABLE 4**). These results reinforce the prognostic value of GPX4 in patients with ICC after surgical resection.

Experimental Study

20 ***ICC cell lines strongly expressed GPX4 protein***

We initially examined the expression levels of GPX4 in four ICC and one HCC cell lines, and we found that all cell lines strongly expressed GPX4 (**SUPPLEMENTARY FIGURE 2**). Of these, two ICC cell lines with high malignancy, HuCCT-1 [22] and SSP-25 [23] were used in the following experiments.

Next, GPX4 was inhibited by gene silencing using siRNA and RSL3 (a GPX4 inhibitor [24]). Western blot analyses revealed that the protein expression of GPX4 were clearly decreased by RSL3 treatment compared to those by siRNA (**SUPPLEMENTARY FIGURE 3A**). Therefore, we attempted to inhibit GPX4 in subsequent experiments using 10 μ M of RSL3, the most suppressed expression of GPX4 protein. According to the mRNA expression of GPX4, siRNA significantly decreased the mRNA expression of GPX4, and RSL3 was not affected (**SUPPLEMENTARY FIGURE 3B, C**).

10

The role of GPX4 on cell proliferation and migration of ICC cell lines

To validate the prognostic value of GPX4 in patients with ICC, we investigated the pathophysiological role of GPX4 using ICC cell lines.

First, we performed the cell viability assay to distinguish dead and viable cells after RSL3 treatment. The results showed that most of RSL3-treated cells were Calcein-AM positive and there were no significant differences in the ratio of Calcein-AM positive cells between RSL3- and DMSO-treated cells. This result suggested that the effect of RSL3 under the condition of this study should be interpreted regarding tumorigenesis in viable cells (**FIGURE 2A**). Next, the WST-8 assay was performed to evaluate the inhibitory effect of GPX4 on cell proliferation. To assess the cell proliferation, cells were treated with RSL3 or DMSO for 72 h, and found that the cell proliferation was significantly suppressed by RSL3 at concentrations in 1 and 10 μ M (**SUPPLEMENTARY FIGURE 4**). We also assessed the cell proliferation by treating RSL3 for 0–72 h and found that treatment with

DMSO increased the cell proliferation over time, whereas treatment with RSL3 for 48 and 72 h significantly suppressed the cell proliferation in both cell lines (**FIGURE 2B**). The cell proliferation was also evaluated by measuring the intracellular DNA content using CyQUANT NF cell proliferation assay kit, and the cell proliferation was significantly suppressed by RSL3 treatment compared to control in both cell lines (**FIGURE 2C**). A wound-healing assay was performed to assess the cell migration, and RSL3 treatment significantly suppressed the cell migration compared to the control (**FIGURE 2D**). To validate the results from *in vitro* studies, the tumor xenograft experiments using HuCCT-1 cells were performed. Tumor growth after RSL3 treatment was significantly suppressed compared with that after treatment with control, and two of the six tumors treated with RSL3 completely disappeared (**FIGURE 2E**). Collectively, these results suggest that the inhibition of GPX4 by RSL3 suppresses tumor growth in ICC cells.

Inhibition of GPX4 suppressed glucose metabolism in ICC cells

Based on the clinical data, we hypothesized that GPX4 involved in cancer-specific glucose metabolism and affected the changes of *GLUT1*, *HIF1 α* or other glucose metabolism-related genes. The results showed that RSL3 treatment significantly downregulated the mRNA expression of *GLUT1* and *HIF1 α* in both cell lines (**FIGURE 3A**). Furthermore, lactate dehydrogenase (*LDHA*), a rate-limiting enzyme involved in the Warburg effect, was significantly downregulated by RSL3 treatment in HuCCT-1 cells (**FIGURE 3A**). Two rate-limiting enzymes of gluconeogenesis, phosphoenolpyruvate carboxykinase 1 (*PCK1*) and glucose 6-phosphatase (*G6PC*), were also examined, and *PCK1* in HuCCT-1 cells was significantly upregulated after RSL3 treatment (**FIGURE 3A**). Similar results were obtained from the western blot analyses. The protein expression of GLUT1 and HIF1 α were suppressed by RSL3 treatment (**FIGURE 3B**). These molecular changes were consistent with the results of the tumor

xenograft model. The IHC analyses of subcutaneous tumors showed that RSL3 treatment downregulated the protein expression of GPX4 and GLUT1 (**FIGURE 3C**). Together with *in vitro* and *vivo* data, GPX4 might have the potential to promote the reprogramming of cancer-specific glucose metabolism in ICC cells.

5

GPX4-mediated glucose metabolism was regulated in Akt-mTOR axis

To further assess the molecular mechanism of GPX4-mediated glucose metabolism, we focused on mechanistic targets of rapamycin (mTOR) signaling. As previous studies have shown, some interactions may exist between GPX4 and Akt-mTOR axis [11, 25-28]. Furthermore, several studies
10 have indicated the interactions between mTOR signaling cascade and ¹⁸FDG uptake or GLUT1 expression [29-31]. In particular, an association between the phosphorylation of ribosomal protein S6 (S6) and the expression of GLUT1 has been identified [32]. These findings prompted us to explore the mechanism regulating GLUT1 expression via Akt-mTOR axis in ICC cells.

We initially sought to determine whether the inhibition of GPX4 by RSL3 affected the
15 activation of mTOR signaling. Notably, RSL3 treatment suppressed GPX4 protein levels and attenuated the phosphorylation of eukaryotic translation inhibition factors 4E-binding protein 1 (4EBP1) and S6, which were the downstream of mTOR signaling (**FIGURE 4A**). RSL3 treatment also inhibited the phosphorylation of Akt (**FIGURE 4A**). These results suggest that GPX4 interacts with Akt-mTOR axis in ICC cells.

20 Next, the inhibitory effects of mTOR signaling using AZD were investigated to clarify the interaction between GPX4 and mTOR signaling in more detail. AZD is an ATP-competitive mTOR inhibitor that inhibits the phosphorylation of 4EBP1 and S6 [33], and we confirmed that AZD

significantly suppressed the cell proliferation of both cell lines (**SUPPLEMENTARY FIGURE 5**). The WST-8 assay after treatment with RSL3, AZD, and their combination revealed that each reagent significantly suppressed the cell proliferation compared to the control in both cell lines. However, no significant differences were observed in the cell proliferation between RSL3 alone, AZD alone, and their combination (**FIGURE 4B**). Consistently, western blot analyses showed that the phosphorylation of 4EBP1 and S6 was equally suppressed by treatment with RSL3 alone, AZD alone, and their combination in both cell lines (**FIGURE 4C**). Meanwhile, GPX4 protein was retained at levels equivalent to those of the control after treatment with AZD (**FIGURE 4C**). Finally, we evaluated the effect of MHY, a mTOR activator on cell proliferation and protein expression. The WST-8 assay showed that the inhibitory effect of RSL3 on cell proliferation was significantly recovered after treatment with the combination of MHY and RSL3 (**FIGURE 4D**). These results were consistent with the western blot analyses. The attenuation of phosphorylation of 4EBP1 and S6 induced by RSL3 was clearly upregulated after co-incubation with MHY and RSL3 (**FIGURE 4E**). Additionally, GLUT1 expression suppressed by RSL3 was clearly upregulated after co-incubation with MHY and RSL3 (**FIGURE 4E**). Our data, therefore, suggested that GPX4-mediated glucose metabolism in cancer cells might be regulated in an Akt-mTOR axis.

DISCUSSION

This study assessed the prognostic relevance of GPX4 and its underlying molecular mechanisms in patients with ICC, from both clinical and experimental perspectives. In the clinical study using surgical specimens, GPX4 expression exhibited significant associations with tumor multiplicity, and SUVmax by ¹⁸F-FDG-PET, and GLUT1 expression with trend towards significance. In this setting, GPX4 overexpression correlated with poorer overall OS and RFS in patients with ICC after surgical resection,

suggesting its potential as a prognostic indicator. In the experimental study, inhibiting GPX4 markedly suppressed cell proliferation and migration, indicating its likely involvement in tumorigenesis. Consistent with the clinical findings, GPX4 inhibition notably affected the expression of glucose metabolism-related genes. Furthermore, these molecular changes were regulated in the Akt-mTOR
5 axis.

Given the increasing interest of ferroptosis and ferroptosis-related gene GPX4, we investigated the impact of GPX4 on survival outcomes in patients with ICC after surgical resection. Consistent with the data of other malignancies, expression level of GPX4 in surgical specimen stratified both OS and RFS. To test the findings of clinical study *in vitro*, we used RSL3-treated ICC cell
10 lines, which specifically decreased the expression of GPX4 [24], because of the limited knock-down effect by the two different siRNA transfection. In this setting, cell proliferation and migration assay *in vitro* were derived from variable cells (**FIGURE 2A**), and it is likely to interpret these data might reflect tumor progression rather than ferroptosis. On the other hand, it should be noted that ferroptosis might have some contributions to the anti-tumor effects of RSL3 *in vivo* models.

15 For further assessing the underlying molecular mechanism in tumor progression, we focused on glucose metabolism because GPX4 expression was closely associated with SUVmax by ¹⁸F-FDG-PET (i.e., representative surrogate for glucose metabolism) in clinical study. Further, GLUT1 expression was associated with GPX4 expression, reinforcing the promising correlation between GPX4 and glucose metabolism. Generally, augmented glucose uptake is one of the features of cancer
20 cells, and the Warburg effect, known as cancer-specific glycolysis, does not involve mitochondrial respiration and supports energy synthesis by generating lactate [34]. In this process, upregulated LDHA preferentially reduces pyruvate to lactate, resulting in promoting cell growth and migration even under hypoxic conditions [35]. Moreover, previous study demonstrated that the overexpression

of PCK1 significantly suppresses tumorigenesis in HCC [36]. In this study, the inhibition of GPX4 not only led to the suppress of the expression of *GLUT1*, *HIF1 α* , and *LDHA* but also upregulated the expression of *PCK1*. These alterations associated with glucose metabolism suggest that GPX4 plays a role in the reprogramming of cancer-specific glucose metabolism, thereby promoting tumor progression in cancer cells. To the best of our knowledge, this is the first study to demonstrate the clinical implications of GPX4 expression associated with ¹⁸F-FDG-PET and GPX4-mediated glucose metabolism.

In the previous studies, interactions between GPX4 and Akt-mTOR axis were reported and RSL3 treatment promoted the suppression of mTOR signaling, such as the activation of S6 and 4EBP1 [26, 27]. Additionally, a significant association between GLUT1 expression and the activation of S6 was identified [32]. These findings prompted us to explore whether GPX4-mediated glucose metabolism was regulated in Akt-mTOR axis. From the results of experimental study, GPX4 expression was clearly associated with the activation of Akt-mTOR axis. Further, our data also showed that GPX4 expression after treatment with mTOR inhibitor was not suppressed compared to those of RSL3. Regarding to the interactions between GPX4 and mTOR signaling, there was controversy as to which was the upstream signaling factor, with some reports suggesting the synthesis of GPX4 was subjected to the activation of mTOR signaling [11, 28]. However, our data indicated that the inhibition of mTOR signaling did not affect the GPX4 expression, providing the hypothesis that GPX4 might be located upstream of mTOR signaling. Moreover, this study identified that the suppression of GLUT1 expression by RSL3 was notably recovered after the activation of Akt-mTOR axis, which was consistent with the previous study [32]. Collectively, these results suggest that GPX4-mediated glucose metabolism might be regulated in Akt-mTOR axis. When testing this hypothesis in phenotype through a cell proliferation assay, the cell proliferation activity by GPX4 in HuCCT-1 cells depended

on mTOR signaling, whereas in SSP-25 cells, it did not. It should be noted that the cell proliferation in SSP-25 cells might be partially attributed to GPX4-mediated glucose metabolism; however, the involvement of other pathways in cell proliferation could not be ruled out.

One of the relevant issues is how these results applied into GPX4-targeted therapy to improve the unsatisfactory survival outcomes of ICC. Despite the recent developments in chemotherapy, effective regimens for ICC are yet to be limited and novel anti-cancer therapy might provide benefits in patients with ICC. Principally, GPX4 functioned in the regulation of intracellular oxidative stress and mediated the induction of ferroptosis [9]. In addition, accumulating evidence suggested that both direct and indirect inhibition of GPX4 induced ferroptosis in several cancer cell lines [11, 37-42]. Intriguingly, several studies have reported that sorafenib and lenvatinib suppressed the expression of System Xc⁻ and reduced intracellular glutathione content. Consequently, GPX4 was indirectly inhibited and ferroptosis was induced in HCC cells [43-45]. These results indicated that ferroptosis-targeted therapeutic strategy might be effective as a novel anti-cancer approach. Crucially, GPX4 functioned not only an inducer of ferroptosis, but also mediated several factors involved in tumorigenesis. While this study did not specifically investigate the anti-cancer effect of ferroptosis *in vitro* studies, GPX4 was considered one of the mediators of glucose metabolism regulated in Akt-mTOR axis. Therefore, targeting GPX4 might expected to have a synergistic effect through the inhibition of glucose metabolism and Akt-mTOR axis, as well as a direct anti-cancer effect through the induction of ferroptosis.

One of the limitations of this study was that the clinical study was a retrospective study from single institution and some biases might be present. Furthermore, there were no external validation cohorts in the clinical study, and we validated the prognostic impact of GPX4 using *in vitro* and *vivo* experiments. Another limitation of this study was that the experiments using knock-down or over-

expression of GPX4 in ICC cells could not be performed due to the low transfection efficacy or absence of GPX4 low expression cells in available ICC cell lines.

In conclusion, this study suggested the pivotal value of GPX4 serving as a prognostic marker for patients with ICC. Furthermore, GPX4 can mediate glucose metabolism of ICC.

5

10

15

20

DECLARATIONS

Conflict of interest declaration:

The all authors have no conflicts of interest to declare.

5 Statements of financial support:

This study was financially supported by Grants-in-Aid KAKENHI (Grant Number 21K1643). It was also supported by the Public Trust Surgery Research Fund (2021) and the Kyoto Healthcare Society Foundation (2022–2023).

10 Author Contributions:

Study conception and design: YH and TY; Material preparation and data collection: YH, TY, HN, KO, MK, YT, MS, TN, YK, TI, and SS; Analysis and interpretation of data: YH, TY, HN, TN, YK, KI, and SS; Writing and revision of the manuscript: YH and TY; Study supervision: EH.

15 Data Availability Statement:

The datasets generated and analyzed in the current study are available from the corresponding author upon reasonable request.

REFERENCES

- 1 Florio AA, *et al.* (2020) Abdominal and gluteofemoral size and risk of liver cancer: the liver cancer pooling project. *Int J Cancer.*, **147**, 675–85.
- 2 Valle JW, *et al.* (2021) Biliary tract cancer. *Lancet.*, **397**, 428–44.
- 5 3 Wu L, *et al.* (2019) Trends in the incidence, treatment and outcomes of patients with intrahepatic cholangiocarcinoma in the USA: facility type is associated with margin status, use of lymphadenectomy and overall survival. *World J Surg.*, **43**, 1777–87.
- 4 Yoh T, *et al.* (2016) Is surgical resection justified for advanced intrahepatic cholangiocarcinoma? *Liver Cancer.*, **5**, 280–9.
- 10 5 Primrose JN, *et al.* (2019) Capecitabine compared with observation in resected biliary tract cancer (BILCAP): a randomised, controlled, multicentre, phase 3 study. *Lancet Oncol.*, **20**, 663–73.
- 6 Nakachi K, *et al.* (2023) Adjuvant S-1 compared with observation in resected biliary tract cancer (JCOG1202, ASCOT): a multicentre, open-label, randomised, controlled, phase 3 trial. *Lancet.*, **401**, 195–203.
- 15 7 Dixon SJ, *et al.* (2012) Ferroptosis: an iron-dependent form of nonapoptotic cell death. *Cell.*, **149**, 1060–72.
- 8 Stockwell BR, *et al.* (2017) Ferroptosis: A regulated cell death nexus linking metabolism, redox biology, and disease. *Cell.*, **171**, 273–85.
- 9 Li J, *et al.* (2020) Ferroptosis: past, present and future. *Cell Death Dis.* in press, doi: 10.1038/s41419-
20 020-2298-2.

- 10 Zhao L, *et al.* (2021) Apatinib induced ferroptosis by lipid peroxidation in gastric cancer. *Gastric Cancer.*, **24**, 642–54.
- 11 Zhang Y, *et al.* (2021) mTORC1 couples cyst(e)ine availability with GPX4 protein synthesis and ferroptosis regulation. *Nat Commun.* in press, doi: 10.1038/s41467-021-21841-w.
- 5 12 Asperti M, *et al.* (2021) H-ferritin suppression and pronounced mitochondrial respiration make Hepatocellular Carcinoma cells sensitive to RSL3-induced ferroptosis. *Free Radic Biol Med.*, **169**, 294–303.
- 13 Yoh T, *et al.* (2019) Reappraisal of prognostic impact of tumor SUVmax by ¹⁸F-FDG-PET/CT in intrahepatic cholangiocarcinoma. *World J Surg.*, **43**, 1323–31.
- 10 14 Chun YS, *et al.* (2018) 8th Edition of the AJCC Cancer Staging Manual: pancreas and Hepatobiliary Cancers. *Ann Surg Oncol.*, **25**, 845–7.
- 15 Clavien PA, *et al.* (2009) The Clavien-Dindo classification of surgical complications: five-year experience. *Ann Surg.*, **250**, 187–96.
- 16 Yoh T, *et al.* (2016) Significant improvement in outcomes of patients with intrahepatic
15 cholangiocarcinoma after surgery. *World J Surg.*, **40**, 2229–36.
- 17 Yoh T, *et al.* (2017) A novel biomarker-based preoperative prognostic grading system for predicting survival after surgery for intrahepatic cholangiocarcinoma. *Ann Surg Oncol.*, **24**, 1351–7.
- 18 Mazumdar M, *et al.* (2000) Categorizing a prognostic variable: review of methods, code for easy
20 implementation and applications to decision-making about cancer treatments. *Stat Med.*, **19**, 113–32.
- 19 Sakamoto Y, *et al.* (2016) Proposal of a new staging system for intrahepatic cholangiocarcinoma: Analysis of surgical patients from a nationwide survey of the Liver Cancer Study Group of Japan. *Cancer.*, **122**, 61-70.

- 20 Denko NC.(2008) Hypoxia, HIF1 and glucose metabolism in the solid tumour. *Nat Rev Cancer.*, **8**, 705–13.
- 21 Baschnagel AM, *et al.* (2015) The association of (18)F-FDG PET and glucose metabolism biomarkers GLUT1 and HK2 in p16 positive and negative head and neck squamous cell carcinomas. *Radiother Oncol.*, **117**, 118–24.
- 22 Miyagiwa M, *et al.* (1989) A new human cholangiocellular carcinoma cell line (HuCCT-1) producing carbohydrate antigen19/9 in serum-free medium in serum-free medium. *In Vitro Cell Dev Biol.*, **25**, 503–10.
- 23 Enjoji M, *et al.* (1997) Hepatocytic phenotypes induced in sarcomatous cholangiocarcinoma cells treated with 5-azacytidine. *Hepatology.* **26**, 288–94.
- 24 Dächert J, *et al.* (2016) RSL3 and erastin differentially regulate redox signaling to promote Smac mimetic-induced cell death. *Oncotarget.*, **7**, 63779–92.
- 25 Hu Z, *et al.* (2023) miR-21-5p inhibits ferroptosis in hepatocellular carcinoma cells by regulating the AKT/mTOR signaling pathway through MELK. *J Immunol Res.* In press, doi: 10.1155/2023/8929525. eCollection 2023.
- 26 Liu Y, *et al.* (2021) Interplay between MTOR and GPX4 signaling modulates autophagy-dependent ferroptotic cancer cell death. *Cancer Gene Ther.*, **28**, 55–63.
- 27 Sekhar KR, *et al.* (2022) Glutathione peroxidase 4 inhibition induces ferroptosis and mTOR pathway suppression in thyroid cancer. *Sci Rep.* In press, doi: 10.1038/s41598-022-23906-2.
- 28 Yan Y, *et al.* (2021) A mTORC1-mediated cyst(e)ine sensing mechanism governing GPX4 synthesis and ferroptosis. *Mol Cell Oncol.* In press, doi: 10.1080/23723556.2021.1919006.

- 29 An J, *et al.* (2022) PET-based radiogenomics supports mTOR pathway targeting for hepatocellular carcinoma. *Clin Cancer Res.*, **28**, 1821–31.
- 30 Bao YY, *et al.* (2022) Effect of Glut-1 and HIF-1 α double knockout by CRISPR/CAS9 on radiosensitivity in laryngeal carcinoma via the PI3K/Akt/mTOR pathway. *J Cell Mol Med.*, **26**, 2881–
5 94.
- 31 Guo XH, *et al.* (2021) Berberine exerts its antineoplastic effects by reversing the Warburg effect via downregulation of the Akt/mTOR/GLUT1 signaling pathway. *Oncol Rep.* doi: 10.3892/or.2021.8204.
- 32 Hirashita T, *et al.* (2020) S6 ribosomal protein phosphorylation is associated with malignancy of
10 intraductal papillary mucinous neoplasm of the pancreas. *Ann Gastroenterol Surg.*, 2020;4:571–9.
- 33 Chresta CM, *et al.* (2010) AZD8055 is a potent, selective, and orally bioavailable ATP-competitive mammalian target of rapamycin kinase inhibitor with in vitro and in vivo antitumor activity. *Cancer Res.*, **70**, 288–98.
- 34 Warburg O. (1956) On the origin of cancer cells. *Science.*, **123**, 309–14.
- 15 35 Goetze K, *et al.* (2011) Lactate enhances motility of tumor cells and inhibits monocyte migration and cytokine release. *Int J Oncol.*, **39**, 453–63.
- 36 Liu MX, *et al.* (2018) Metabolic reprogramming by PCK1 promotes TCA cataplerosis, oxidative stress and apoptosis in liver cancer cells and suppresses hepatocellular carcinoma. *Oncogene.*, **37**, 1637–53.
- 20 37 Yang WS, *et al.* (2014) Regulation of ferroptotic cancer cell death by GPX4. *Cell.*, **156**, 317–31.
- 38 Roh JL, *et al.* (2016) Induction of ferroptotic cell death for overcoming cisplatin resistance of head and neck cancer. *Cancer Lett.*, **381**, 96–103.

- 39 Eling N, *et al.* (2015) Identification of artesunate as a specific activator of ferroptosis in pancreatic cancer cells. *Oncoscience.*, **2**, 517–32.
- 40 Galmiche A, *et al.* (2014) New biological perspectives for the improvement of the efficacy of sorafenib in hepatocellular carcinoma. *Cancer Lett.*, **346**, 159–62.
- 5 41 Louandre C, *et al.* (2015) The retinoblastoma (Rb) protein regulates ferroptosis induced by sorafenib in human hepatocellular carcinoma cells. *Cancer Lett.*, **356**, 971–7.
- 42 Hasegawa M, *et al.* (2016) Functional interactions of the cystine/glutamate antiporter, CD44v and MUC1-C oncoprotein in triple-negative breast cancer cells. *Oncotarget.*, **7**, 11756–69.
- 43 Xu FL, *et al.* (2023) SLC27A5 promotes sorafenib-induced ferroptosis in hepatocellular carcinoma
10 by downregulating glutathione reductase. *Cell Death Dis.* In press, doi: 10.1038/s41419-023-05558-
w.
- 44 Tang H, *et al.* (2019) Dual GSH-exhausting sorafenib loaded manganese-silica nanodrugs for inducing the ferroptosis of hepatocellular carcinoma cells. *Int J Pharm.* In press, doi: 10.1016/j.ijpharm.2019.118782.
- 15 45 Iseda N, *et al.* (2022) Ferroptosis is induced by lenvatinib through fibroblast growth factor receptor-4 inhibition in hepatocellular carcinoma. *Cancer Sci.*, **113**, 2272–87.

TABLE AND FIGURE LEGENDS

TABLE 1.

Clinicopathological characteristics according to GPX4 expression.

TABLE 2.

5 Association of GPX4 expression with ¹⁸F-FDG uptake and GLUT1 expression.

FIGURE 1.

Prognostic impact of GPX4 expression in patients with ICC after surgical resection. **A**, Representative IHC images of GPX4 expression in surgical specimens of ICC. **B**, Representative images indicating the
10 associations between SUVmax and GPX4 expression. **C** and **D**, Kaplan-Meier analyses for OS (**C**) and RFS (**D**) in 57 patients with ICC according to GPX4 expression levels.

FIGURE 2.

Pathophysiological role of GPX4 on tumorigenesis in ICC cells. **A**, Cell viability assay revealed that
15 most of cells after treating with RSL3 were viable. **B**, **C** and **D**, WST assay (**B**), CyQUANT NF Cell proliferation assay (**C**) and wound healing assay (**D**) demonstrated that proliferative and migratory potential were significantly suppressed by RSL3 treatment in both ICC cell lines. **E**, RSL3 treatment attenuated tumor growth in tumor xenograft model using HuCCT-1 cells. Data represent the mean ± SD of at least three independent experiments.

20

FIGURE 3.

Inhibition of GPX4 suppressed glucose metabolism in ICC cells. **A** and **B**, qRT-PCR (**A**) and western blot (**B**) analyses were demonstrated to evaluate the changes of glucose metabolism-related genes and proteins in ICC cells after RSL3 treatment. **C**, Representative IHC images of GPX4 and GLUT1 expression in tumor xenograft model. Data represent the mean \pm SD of at least three independent experiments.

FIGURE 4.

GPX4-mediated glucose metabolism was regulated in Akt-mTOR axis. **A**, Western blot analyses showed that RSL3 treatment clearly suppressed the activation of mTOR signaling cascade. **B** and **C**, WST assays (**B**) and western blot analyses (**C**) were performed after treating with RSL3, AZD8055 and its combination therapy. **D**, MHY1485 significantly recovered the inhibitory effect of cell proliferation induced by RSL3. **E**, The protein expression of p-4EBP1, p-S6 and GLUT1 was clearly upregulated after treating with MHY1485 and RSL3 combination therapy. Data represent the mean \pm SD of at least three independent experiments.

TABLE 1.

Clinicopathological characteristics according to GPX4 expression.

Overall (n=57)	GPX4 High (n=15)	GPX4 Low (n=42)	
Variables			<i>p</i> value
Age (years), median, range	73 (48-83)	69 (32-84)	0.151
Sex male, n (%)	6 (40.0)	27 (64.3)	0.103
Hepatitis B, n (%)†	2 (14.3)	1 (2.5)	0.161
Hepatitis C, n (%)†	4 (26.7)	2 (4.76)	0.036*
CEA (ng/ml), median, range	3.6 (0.9-87.8)	3.8 (0.4-133.1)	0.685
CA19-9 (IU/ml), median, range	23.6 (0.6-574.5)	55.9 (0.6-3055.0)	0.161
Tumor diameter (cm), median, range	3.2 (1.5-13.0)	3.7 (1.1-14.0)	0.599
Multiple tumors, n (%)	8 (53.3)	6 (14.2)	0.004*
Major biliary invasion, n (%)	6 (40.0)	18 (42.9)	0.847
Microvascular invasion, n (%)	9 (60.0)	27 (64.3)	0.766
LN metastasis, n (%)			0.370
N1	3 (20.0)	14 (33.3)	
N0	9 (60.0)	25 (59.5)	
Nx	3 (20.0)	3 (7.2)	
Poorly differentiation	4 (26.7)	9 (21.4)	0.727
AJCC T3/4, n (%)	9 (60.0)	24 (57.1)	0.847
AJCC Stage III/IV, n (%)	11 (73.3)	25 (59.5)	0.333
Adjuvant chemotherapy, n (%)	10 (66.7)	26 (61.9)	0.742
Major hepatectomy, n (%)	13 (86.7)	37 (88.1)	0.886
R0 resection, n (%)	13 (86.7)	36 (85.7)	0.927
C-D grade \geq II, n (%)	4 (26.7)	12 (28.6)	1.000

* Significant difference

†: Fisher's exact test was used.

Abbreviations: GPX4, glutathione peroxidase 4, CEA; carcinoembryonic antigen, CA19-9; carbohydrate antigen 19-9, SUV; standardized uptake value, LN; lymph node, AJCC; American Joint Committee on Cancer, C-D; Clavien-Dindo classification.

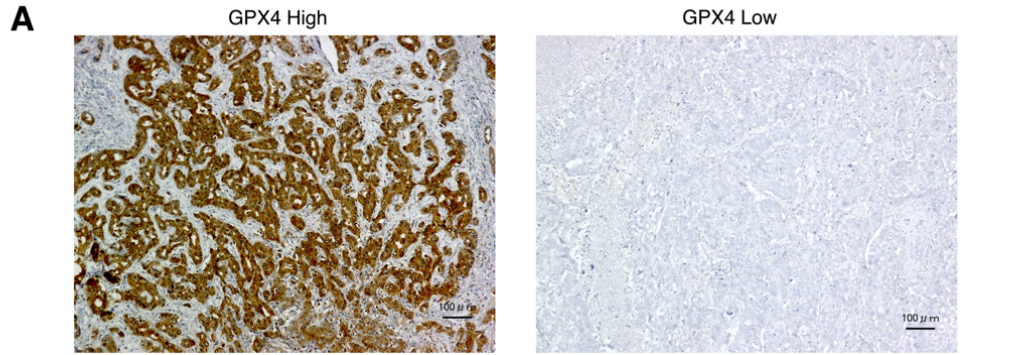
TABLE 2.Association of GPX4 expression with ¹⁸F-FDG uptake and GLUT1 expression.

Overall (n=57)	GPX4 High (n=15)	GPX4 Low (n=42)	
Variables			<i>p</i> value
SUVmax ≥ 8.0, n (%)†	9 (69.2)	12 (31.6)	0.017*
SUVmax, median, range †	8.4 (3.4-13.8)	6.6 (2.6-14.7)	0.059
GLUT1 score high, n (%)	12 (80.0)	22 (52.4)	0.053

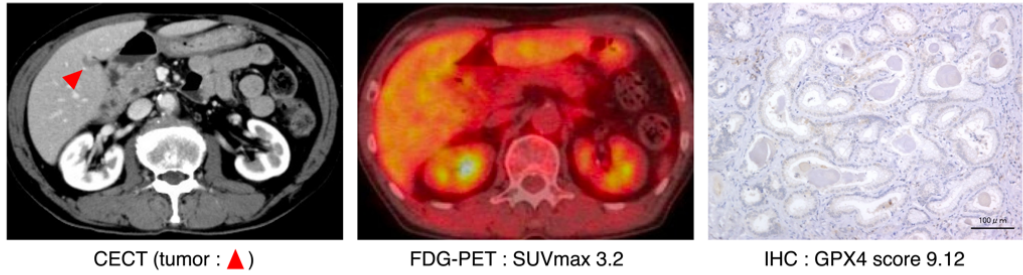
* Significant difference

†: Using 51 patients for whom data of ¹⁸F-FDG-PET were available (GPX4 high; n=13, GPX4 low; n=38)Abbreviations: GPX4, glutathione peroxidase 4, ¹⁸F-FDG ; ¹⁸F-fluorodeoxyglucose, GLUT1; glucose transporter 1.

FIGURE 1



B Representative images of SUVmax low and GPX4 low case.



Representative images of SUVmax high and GPX4 high case.

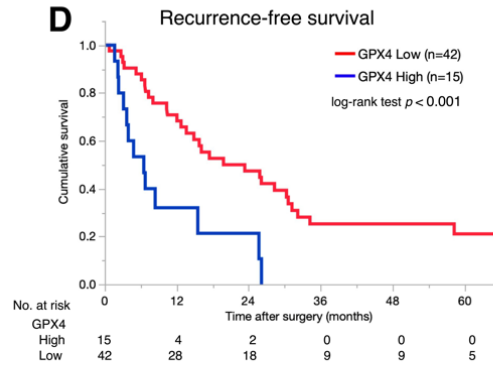
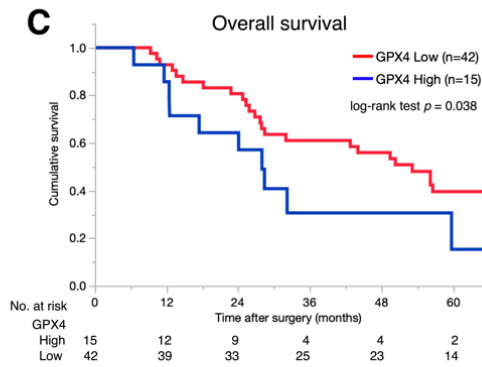
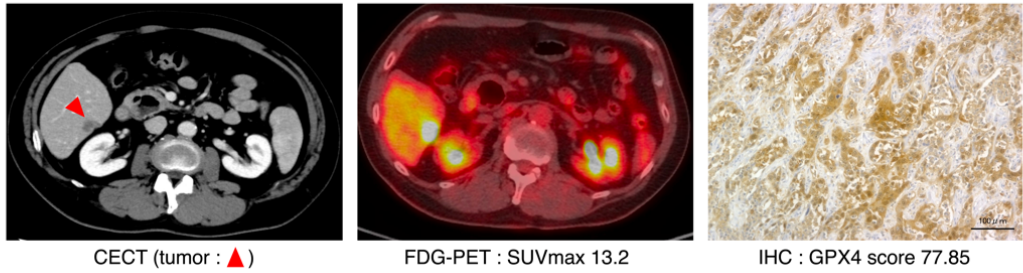


FIGURE 2

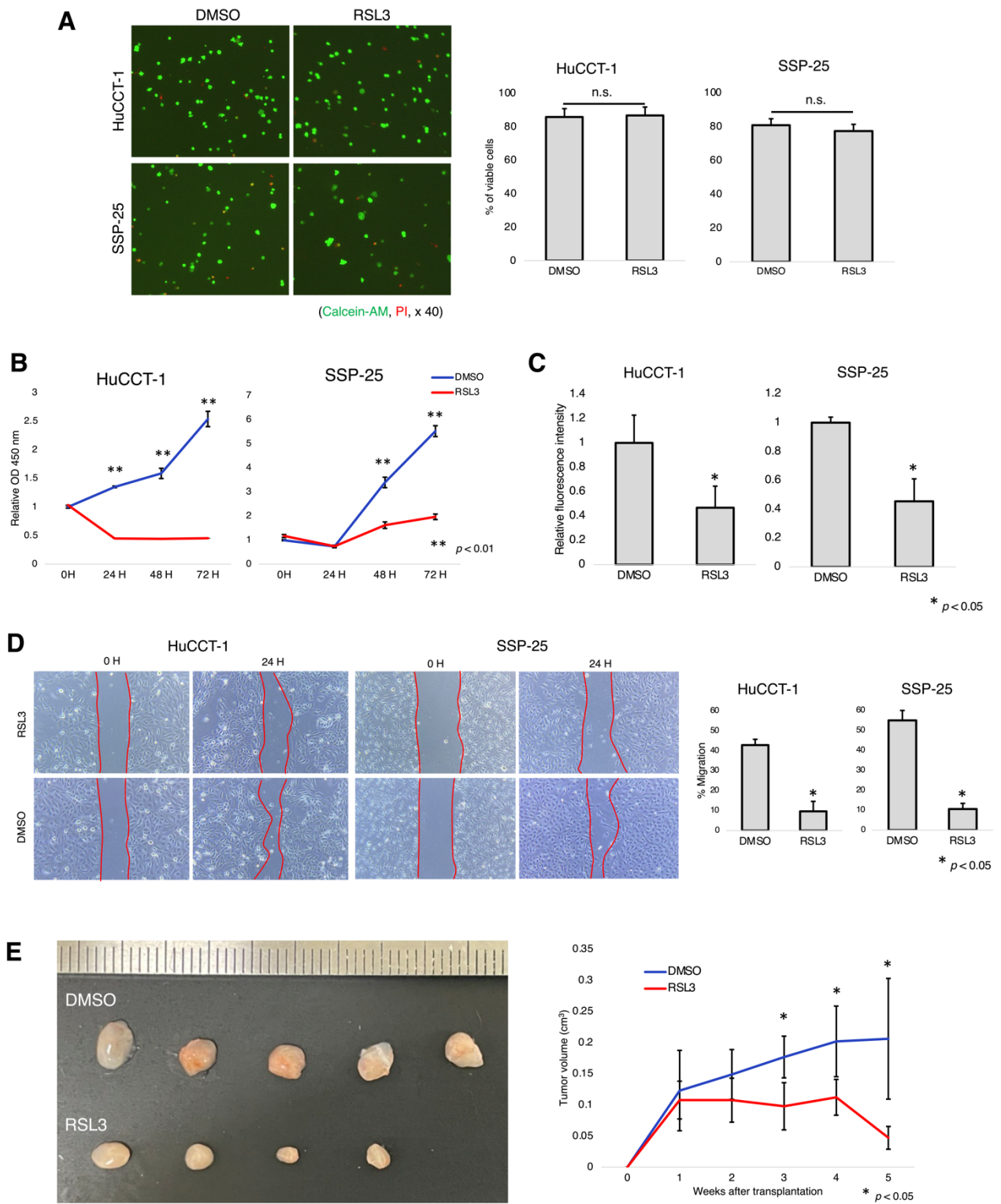


FIGURE 3

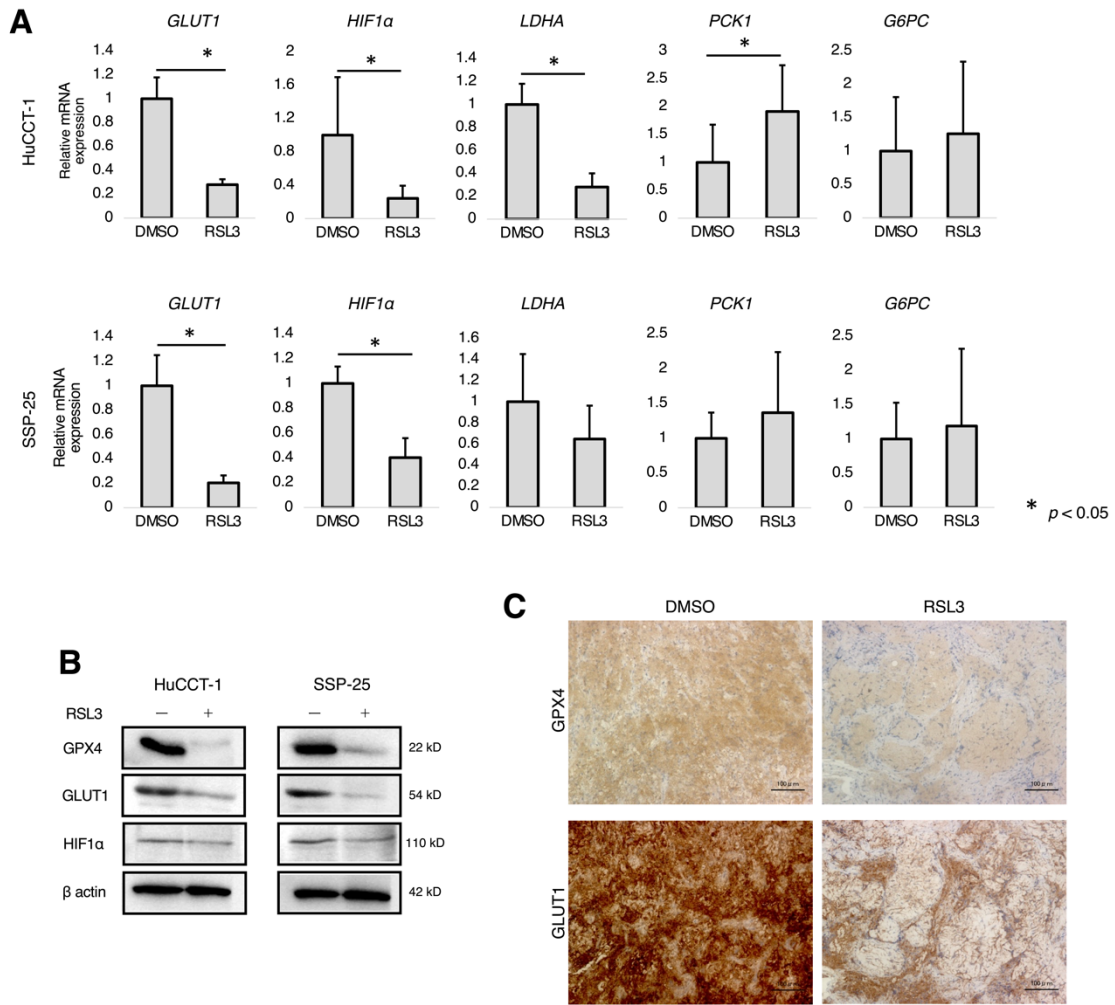


FIGURE 4

